J Mater Sci: Mater Med (2008) 19:1971–1979
DOI 10.1007/s10856-007-3274-4

# Estimation of the strength of adhesion between a thermoresponsive polymer coating and nitinol wire

**Martin Burke · Brenda Clarke · Yuri Rochev · Alexandar Gorelov · William Carroll**

Received: 8 May 2006 / Accepted: 5 September 2007 / Published online: 18 October 2007


**Abstract** As polymer coatings become more widely used in the biomedical device industry, both to improve biocompatibility and as coatings for localised drug delivery, quantitative methods to measure the adhesive strength between coatings and substrates become a very important consideration. The aim of this study was to take a method for estimating the interfacial fracture toughness of a film to a flat substrate and apply it to Nitinol wires used in the production of medical devices. An investigation into the affect of surface roughness on the fracture toughness was also conducted. For the present study, a thermoresponsive based Poly (*N*-isopropylacrylamide) polymer was coated onto nitinol wire substrates and the adhesion strength between the polymer and wire was measured using a nanoindentation technique. Different surface treated nitinol wires, with different surface topography and roughness were used, and the affect of these surface properties on adhesion strength was investigated. Results showed that it was possible to apply the delamination technique to wire samples and obtain fracture toughness values. Results also showed that the surface roughness is an important parameter that can affect the adhesion between a coating and the substrate. It was found that, as the average surface roughness increased so also did the adhesive strength between the coating and wire sample.

M. Burke (✉) · B. Clarke · Y. Rochev · W. Carroll
National Centre for Biomedical Engineering Science, National University of Ireland, Galway, Ireland
e-mail: mairtin.deburca@gmail.com

A. Gorelov
Department of Chemistry, University College Dublin, Dublin, Ireland

## 1 Introduction

With the ever-expanding use of polymer coatings in the biomedical industry, the need for methods to study how a coating interacts with the substrate becomes increasingly important. This is especially true in relation to polymer coatings for drug eluting stents. There are a number of problems associated with stent coatings. Coating imperfections can result in poor biocompatibility and an increased risk of restenosis. These imperfections may be uneven coating thickness, non-uniform roughness, or delamination. These imperfections can be due to a number of reasons, such as the coating technology used, stent crimping, delivery of the stent to the occluded site, or expansion of the stent. Delamination results when the polymer coating separates from the substrate, and may occur due to residual stress induced crack growth between the film and substrate [1]. Delamination is caused by poor adhesion of the polymer coating to the substrate. This debonding that can occur, may significantly affect the performance and reliability of devices [2].

Delamination of the stent coating can lead to exposure of the metal substrate. This may result in thrombus formation and acute occlusion of the artery [3]. Debonding of the stent coating can also result in debris floating in the blood stream, and this can cause further adverse immunological responses. Delamination may cause a change in the drug elution profile from the stent coatings. An increased rate of elution from the coating may mean a shorter treatment period, or may result in non-localised delivery of the drug if the flakes are carried away in the blood. This can all result in decreased levels of drug at the damaged site, which in turn could lead to failure to prevent restenosis.

There is a high risk of delamination occurring with polymer-coated stents as a consequence of delivery of the stent to the diseased site and subsequent expansion of the stent. A suitable stent coating must, therefore, be able to withstand a certain amount of stresses prior to expansion. They must adhere strongly enough to the substrate not to delaminate during or after expansion. There is, therefore, a need to be able to measure the adhesive strength of a polymer coating to a substrate to establish its suitability as a coating for a drug delivery stent.

There are a large number of techniques available for measuring the strength of adhesion between films and substrates. These techniques include scratch tests [1], pullout tests [4], and techniques, which involve Atomic Force Microscopy [5]. While a large number of techniques have been employed for measuring adhesive strength, indentation induced delamination is one of the most common ways of measuring the interfacial fracture toughness between thin films and metal substrates. The indentation method was first proposed by Chiang et al. and later developed by a number of groups [6]. Advantages of the technique include, no sample preparation required, hardness testing machine and optical microscope are the only instruments needed and reproducible results can be obtained quickly, with minimal damage to samples.

In this study, nanoindentation was used to induce the delamination of a thermoresponsive co-polymer on a number of nitinol wire samples that had received various surface treatments. The fracture toughness was estimated from the size of the delamination zone using the annular-plate analysis method, which was developed for soft compliant films and rigid substrates [2]. Nanoindentation was used as it was considered simpler and more practical than conventional tests such as the peel test or pull off test, due to the impracticalities of performing these tests on micro scale systems such as wires and stents.

Previous studies have reported that surface parameters such as roughness and chemistry can significantly influence adhesion at interfaces [5, 7]. In this study, the topography and roughness of the nitinol wires was analysed and an investigation was carried out to see if surface roughness had an affect on the interfacial fracture toughness.

The use of nitinol (NiTi) as an alternative material to stainless steel and tantalum offers many advantages such as shape memory, superelasticity, and radiopacity [8]. Nitinol is a very useful biomaterial and research has proven it to be both corrosion resistant [9, 10] and biocompatible in both in-vivo [11, 12] and in-vitro [13, 14] environments. Due to the fact that nitinol exhibits superelastic and shape memory properties, if it is coated, the interface must have sufficient strength to transfer stresses and strains to the coated material. This makes the investigation of factors affecting the adhesive strength between nitinol and coatings an important endeavour [4].

The polymer used for the coating of the nitinol wires was the thermoresponsive based Poly (*N*-isopropylacrylamide) (PNIPAAm) polymer. (PNIPAAm) has aroused particular interest because of its potential in drug delivery, enzyme immobilization, surface modification and as a thermosensitive adsorbant [15], due to the abrupt nature of its phase transition, and the closeness of the lower critical solution temperature (LCST) to 37 °C. PNiPAAm has a LCST of approximately 32 °C in an aqueous solution [16]. Below the LCST NiPAAm based polymers are water soluble, while above the LCST they shrink and precipitate out of aqueous solutions. It is possible to load drugs or other active agents into the polymer solutions at temperatures less than the LCST and trap the drug in the polymer by increasing the temperature above the LCST. The drug can then be released in a diffusion-controlled manner [17]. In this study NiPAAm was copolymerised with a more hydrophobic monomer *N-tert*-Butylacrylamide (NtBAAm). Increasing the ratio of NtBAAm in the copolymer reduces the LCST of the copolymer. It has been shown in another study that it is possible to control the release rate of the hydrophobic drug colchicine from the copolymer by varying the amount of NtBAAm in the copolymer [17]. It is this ability to incorporate active agents, and subsequently control the release that has led to this investigation into the possible use of PNiPAAm as a potential coating for drug-eluting coronary stents [18]. Co-polymers of PNiPAAm were chosen because of their biocompatibility, potential as drug delivery vehicles and their similar properties to polystyrene that was used in a study by Li et al [2], from which the numerical model to calculate the adhesive strength in this study was taken.

To date, work measuring the adhesive strength between films and substrates, has been conducted on flat substrates [2, 19–21]. In order to obtain reliable and usable data from a biomedical point of view, it is important to use samples that mirror those used in actual stent production. For this reason, wires and not flat samples were used. As the wires used in this study are similar to those used in the manufacture of stents, the analysis was carried out on real product material. The work carried out in this study is a first, in a sense that stent wire material and not flat substrates are used in this procedure.

## 2 Materials and methods

### 2.1 Nitinol wire substrates

Nitinol wire samples with a diameter of 0.030 inches (0.762 mm) were fabricated from binary nickel–titanium

alloy with a nominal composition of 50.8 atomic percent nickel and an austenite start temperature in the fully annealed condition of –31 °C as measured by DSC per ASTM F 2004-00. All nitinol samples were prepared by Fort Wayne Metals Research Products Corporation, USA, especially for this study. Standard reduction and thermal processing was used to draw the wire to 0.0403 inches (1.02 mm). Additional processing to achieve 45% cold work at 0.030 inches followed by a heat straightening step to produce superelastic properties at room to body temperature were performed. The active $A_f$ temperature of the final wire was measured using the Bend and Free recovery method per ASTM-F 2082-01 to confirm that a superelastic condition had been achieved.

All specimens were cold drawn using either synthetic polycrystalline (Syn.Poly.) diamond dies or single crystal natural diamond (ND) dies. These two dies are used by Fort Wayne Metals in the manufacture of Nitinol wires. Heat straightening was performed at 500 °C under various levels of an argon/oxygen atmosphere. After heat straightening, all of the wires were subjected to additional chemical and/or mechanical treatments in order to achieve the desired surface states.

Removal of the oxide by etching (E) using a proprietary Fort Wayne Metals (FWM) acid solution was performed for a series of specimens with the intent of attacking only the oxide itself. Additional specimens were exposed to a pickling process (P), after the initial etching again using an acid solution of a proprietary nature to FWM. This second chemical exposure allowed attack of the base material. To achieve additional test conditions for the study, specimens that had been etched, or both etched and pickled, were mechanically polished (M) using a mechanical wire polishing machine. The mechanical polishing was also carried out by FWM. The wires were guided through a series of spinning abrasive wheels, to produce a smooth finish. The entire wire surface was mechanically polished. Details of the wire surface preparation procedures are outlined in Table 1. All the samples were cleaned thoroughly using laboratory detergent, sonnicated for 15 min and then rinsed three times in ethanol and water. Samples were left to air dry.

**Table 1** Wire preparation procedures for each sample. ND = Natural diamond die, Syn. Poly. = synthetic polycrystalline die, E = etched, P = Pickled and M = mechanically polished

| Sample | Surface treatment |
|---|---|
| No. 1 | ND/E |
| No. 2 | ND/E/P |
| No. 3 | Syn. Poly/E/P |
| No. 4 | Syn. Poly/E/P/M |
| No. 5 | ND/E/M |

## 2.2 Polymer synthesis

The co-polymer of poly(*N*-isopropylacrylamide) (PNIPAAm) *N-tert*-butylacrylamide (PNtBA) in a ratio of 65:35 was used to coat the nitinol wires. The co-polymer was prepared by free radical polymerization of the corresponding monomers using azobisisobutyronitrile (0.5 mol% of AIBN) as an initiator in benzene (10%, w/w) under argon. After polymerization at 60 °C for 24 h, the mixture was precipitated in hexane. Precipitation was repeated three times using acetone as a solvent and hexane as a non-solvent, and the product was dried at room temperature in a vacuum. The NIPA (97% Aldrich) and NtBA, (purum, Fluka Chemie, Switzerland) were recrystallised from hexane and acetone, correspondingly. 2, 2′-Azobis(2-methylpropionitrile) (AIBN), (Phase Separation LTD, Queensferry, Clyd, UK) was recrystallised from methanol. All other solvents were reagent grade and were dried and distilled before use [17]. The co-polymer structure is shown in Fig. 1.

## 2.3 Wire surface topography

Wire surface topography was analysed using Scanning electron microscopy (SEM). SEM examination of the wire surfaces was carried out using a Hitachi S-4700 field emission microscope at a variety of magnifications ranging from 100× to 10000×

## 2.4 Wire surface roughness

A Veeco Digital Instruments Dimension 3100 atomic force microscope (AFM) was used to measure the surface roughness of the various wire samples. A triangular silicon-nitride tip mounted on a cantilever (Stiffness constant 0.57 N/m) was operated in contact mode. Roughness

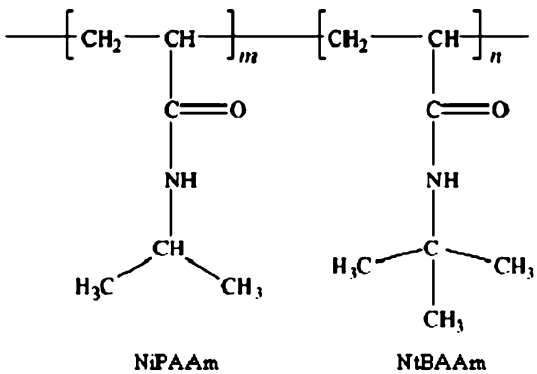


**Fig. 1** The chemical structure of the *N*-isopropylacrylamide (NIPAAm) and *N-tert*-butylacrylamide (NtBA) co-polymer

values were measured from the mean plane within the box cursor of a total scan area of 20 × 20 μm. The width of the box was approximately 2 μm and the length 15 μm and it was aligned on the topmost part of the wire surface and parallel to the wire direction. This is illustrated in Fig. 2, which shows a 20 $\mu m^2$ scan obtained from sample no. 1, the 2 × 15 μm box from where the results were obtained can be seen in the middle of the scan area. The purpose of analysing within this box was to minimise the effect that the wire curvature had on the surface analysis results. Surface roughness was analysed in terms of the $R_a$ and $R_z$ values. The $R_a$ values, or mean roughness, represent the arithmetic average of the deviations from the centre plane. The $R_z$ are the arithmetic averages of the absolute values of the surface height deviations. $R_z$ corresponds to the z range value shown in Fig. 2. Samples were analysed at a rate of 0.5 Hz and each wire sample was randomly scanned in six different locations.

## 2.5 Coating samples

The wire samples were coated with the *N*-isopropylacrylamide (NIPAAm) and *N-tert*-butylacrylamide (NtBAAm) co-polymer in a 65:35 ratio using a 10% solution in ethanol and a Nima dip coater. Coating thickness was controlled by the dip coater withdrawal speed. Each wire received two dips with a withdrawal speed of 80 mm/min. This gave the desired coating thickness of 10 μm. The coated samples were placed in an atmosphere of ethanol for 24 h and dried in an oven at 55 °C overnight. Once samples were dried, the thickness of the coatings was measured using a micrometer. Measurements were taken at three different points along the length of the coated wire and the average thickness calculated.

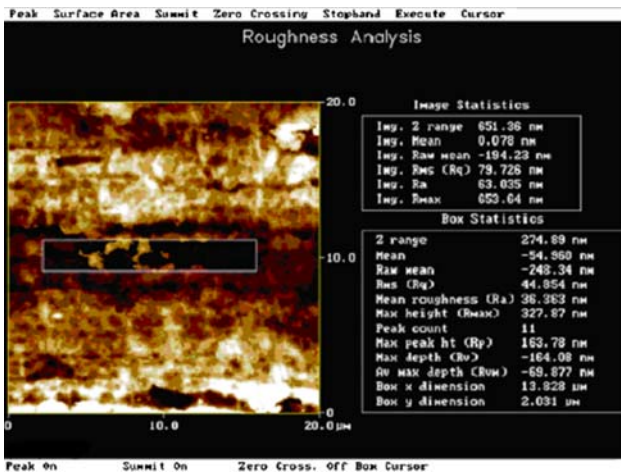


**Fig. 2** AFM image of the surface of a wire sample. The 2 × 15 μm area analysed is outlined in the center of the image. The statistical analysis of the wire surface is given in the boxes beside the image

## 2.6 Nano-indentation induced delamination

Nanoindentation tests were conducted on coated wire samples with a Nanohardness tester (NHT, CSM Instruments, Switzerland) using a spherical diamond indenter, with a tip radius of 10 μm. To ensure delamination occurred, a load of 250 mN applied at a rate of 500 mN/min was used. A suitable area for the indentation on the surface of the sample was chosen using the microscope. The microscope set at ×40 magnification was used to view the indents. A simple indentation was then performed where the sample was indented to a load of 250 mN and then unloaded completely. The sample was then brought back under the microscope where the image of the indent and surrounding delamination were captured using video software. The image was then analysed using NIH Scion Image Software and the radius of the delamination zone was ascertained. The annular plate analysis [2] gives the interfacial fracture toughness or strain energy release rate as:

$$G = \frac{2(1-v^2)(\sigma_{ys}-H)^2 h}{E(1+v+(c/a)^2(1-v))^2}$$

where c is the delamination radius, a is the tip radius; E, H, and v are the elastic modulus, hardness and Poisson's ratio of the film respectively; and h is the film thickness. The yield stress, $\sigma_{ys}$, is estimated from the hardness by $\sigma_{ys} \cong H/2.1$ according to Li et al. [2]. The elastic modulus and hardness of the 65:35 NiPAAm/NtBAAm co-polymer were determined from stress-strain curves obtained using the NHT. These studies were conducted on polymer films that were cast onto flat stainless steel coupons. Poisson's Ratio for the polymer is 0.33. The values for the delamination radius and the tip radius were obtained from analysis of the visible light microscopy images of the circular indentation and resulting delamination, after indentation-induced delamination.

## 2.7 Measurement of the mechanical properties of the polymers

To calculate the interfacial fracture toughness of the polymer to the substrate, the elastic modulus and hardness of the polymer needs to be accurately known. Nanoindentation was used to measure the elastic modulus and hardness of the polymer. The experiments were carried out on films cast on flat substrates using a Nanohardness tester

(NHT, CSM Instruments, Switzerland) with a Berkovich indenter tip. Loads of 3 mN, with a loading rate of 6 mN/min were used for measuring the elastic modulus and hardness of the films in this study. A total of six areas per sample were analysed and the average elastic modulus and hardness values calculated.

## 3 Results and discussion

### 3.1 Surface topography

From the images obtained from the SEM it was clear that the etched and pickled samples were rough and that mechanically polishing of the samples reduced the roughness by a considerable degree. As indicated in Fig. 3a, at a magnification of close to ×10000, the etched and pickled wire surface of sample No.2 is clearly rough. When compared to the etched, pickled and mechanically polished surface of sample No.4, as presented in Fig. 3b at a similar magnification, we can see it is much smoother. At higher magnifications, the same is true. Samples that had been subjected to picking or etching had rough surfaces with deep grooves and defects. The mechanically polished samples appeared smooth, with longitudinal grooves on the surface.

### 3.2 Surface roughness

Both the $R_z$ and $R_a$ roughness values were analysed to obtain as much information about the surface as possible. While the $R_z$ and $R_a$ roughness values are related to each other, the $R_z$ roughness averages the highest and deepest peaks; therefore extremes have a great effect on the final $R_z$ value. This is a good roughness parameter for analysis of metal surfaces, due to the irregularities that result from the preparation procedures. The $R_z$ roughness values and the $R_a$ roughness values are presented in Table 2. SEM images showed that the etched and pickled samples had a rough topography. The AFM results correlate well with this, as the etched surface, No.1 had the roughest surface, with an average $R_z$ roughness of 278 nm. The average surface roughness for the pickled sample No.2 was slightly lower at 268 nm. SEM images showed that mechanical polishing resulted in a smooth surface. Two samples were mechanically polished, one after being etched and the other after being pickled. Mechanically polishing samples after etching and pickling (sample No. 4) reduced the $R_z$ roughness to 145 nm, and to 92 nm after etching (sample No.5). It can be deduced that chemical treatment of nitinol by etching and pickling results in a rough surface, which can be removed and replaced by a smoother surface after additional mechanical treatment such as polishing.

### 3.3 Mechanical properties of the polymer

Figure 4 shows a typical load-displacement curve used for the measurement of the mechanical properties of the different polymers. Using a multicycle like the one shown in Fig. 4 eliminates any reverse plasticity that occurs in the first three loadings and unloadings, while the peak hold allows for any creeping to diminish. By the time the fourth unloading occurs an accurate reading for the elastic modulus is obtained [22].

When measuring the elastic modulus or hardness of film using indentation techniques it is important not to indent to a depth greater than 10% of the total film thickness. At depths greater than this the substrate may begin to influence the results [23]. The film thickness on all samples was 10 μm. Loads of 3 mN resulted in an indentation depth of less than 1 μm. Elastic modulus and hardness values were calculated by the nanoindentation software. The average values of elastic modulus and hardness of 65:35 NiPAAm/NtBAAm copolymer were recorded as 4.20 ± 0.05 GPa and 0.210 ± 0.001 GPa respectively. The calculation of the interfacial fracture toughness relies on a number of experimentally measured variables. The elastic modulus and hardness of the polymer films are two such measured variables. Due to the repeatability of the elastic modulus and hardness results obtained from the polymer films measured using nanoindentation these values were regarded as constants when calculating the interfacial fracture toughness.

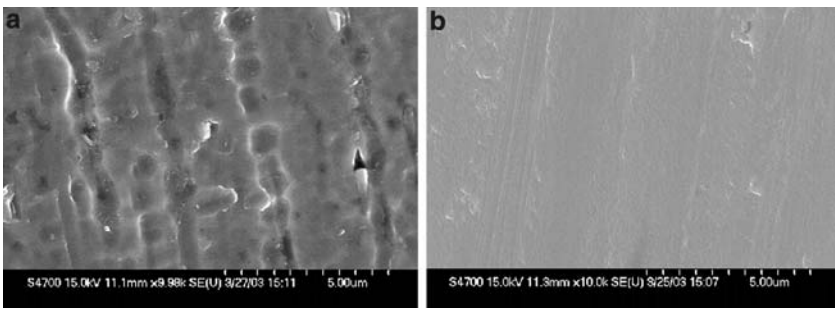


**Fig. 3** (**a**). An SEM image of sample no.2, which was etched and pickled. The magnification is ×10, 000. The surface of the sample is clearly rough. (**b**). An SEM image of sample no.4, which was Mechanically polished. The magnification is ×10, 000. The sample appears to have a smooth surface

**Table 2** The $R_z$ and $R_a$ roughness values, the c/a ratios and the calculated interfacial fracture toughness values for all samples

| Sample no. | $R_z$(nm) | $R_a$ (nm) | c/a | G (J $m^{-2}$) |
|---|---|---|---|---|
| 1 | 278 ± 96 | 34.2 ± 8 | 2 ± 0.04 | 0.32 ± 0.02 |
| 2 | 268 ± 52 | 32.7 ± 8 | 2.21 ± 0.03 | 0.24 ± 0.01 |
| 3 | 230 ± 37 | 25.7 ± 6 | 2.36 ± 0.06 | 0.20 ± 0.02 |
| 4 | 145 ± 47 | 14 ± 2 | 2.96 ± 0.18 | 0.10 ± 0.02 |
| 5 | 92 ± 28 | 10.9 ± 4 | 2.41 ± 0.05 | 0.19 ± 0.01 |

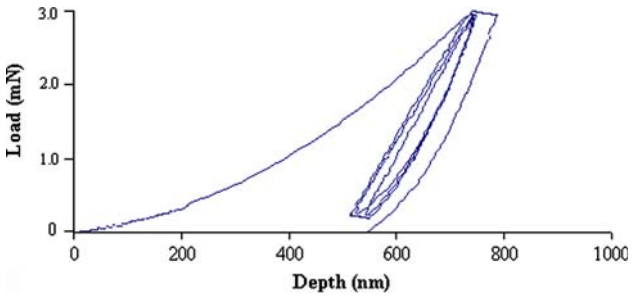


**Fig. 4** A typical stress strain curve from which elastic modulus and hardness were determined. A multicycle indentation with a maximum load of 3 mN was used. The maximum depth reached was approximately 800 nm

### 3.4 Nano-indentation induced delamination

Figure 5a shows an example of the image of indentation and delamination as seen with the microscope of the NHT. Figure 5b shows the same image after it has been analysed using the NIH scion image software. The radius of the indenter tip is indicated by a, and the delamination radius is shown as c. The c/a ratio is the most important parameter that varies when calculating the adhesion strength. A small delamination zone results in a small c/a ratio and indicates strong adhesion, while a larger delamination zone results in a large c/a ratio and represents weaker adhesion to the substrate. The c/a ratios for each sample are given in Table 2. Since these values are measured optically the quality of the image can affect the accuracy of the results, as there can be uncertainty in estimating the edge of the delamination radius. The delamination of the polymer, and the fact that there was a non-transparent substrate made it more difficult to obtain good optical resolution. In this study the radii were measured three times in different areas and the average values taken. The error in measurement of the radii was found to be less than 10%. Interfacial fracture toughness values calculated from the annular plate equation for each wire sample are recorded in Table 2.

Previous work carried out using indentation-induced delamination to measure coating adhesion strength, report observing irregularities in the load-displacement curves [24–28]. Figure 6a shows a typical load-displacement curve obtained from a delamination indentation using a load of 250 mN. There were no obvious irregularities in the loading or unloading curve identifying when the delamination occurred. However, when the indentation was repeated at 100 mN the resulting load-displacement curve showed irregularities in both the loading and unloading curve. Figure 6b shows this curve with the areas of irregularity highlighted and enlarged. The step in the loading curve corresponds to a discontinuity in indenter motion, caused by a sudden advance of the indenter into the material. This indicates, that as the load was increasing and the indenter tip was travelling deeper into the polymer there was a build up of stress in the polymer around the indenter, this stress increased until the polymer structure or interface can no longer withstand it and the polymer buckles or delaminates which releases the build up of stress. It is this release of stress that accounts for the sudden advance of the indenter into the sample and is represented by the step on the loading curve. Again the irregularity on the unloading curve is caused by a discontinuity in indenter motion. Close examination of the enlarged portion shows that as the indenter was withdrawing from the surface at a constant rate it is suddenly forced out rapidly for a brief period. This is due to some recovery of the material

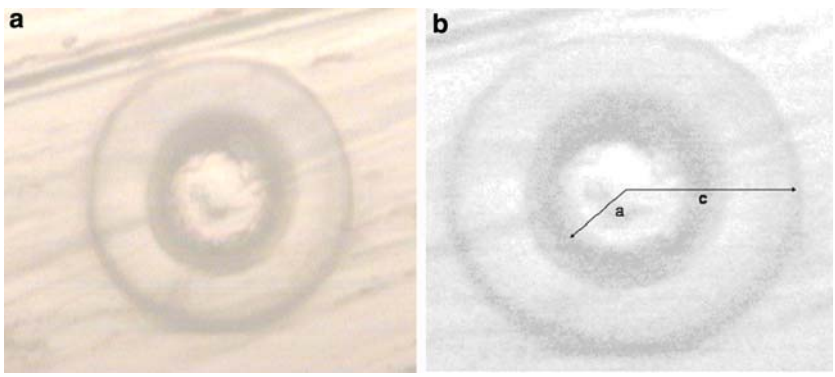


**Fig. 5** (**a**) An Example of the indentation induced delamination as captured with the visible light microscope of the NHT. The magnification used was ×40. (**b**) Indentation induced delamination image after it has been analysed using the NIH scion image software. The indentation radius is indicated by a, and the delamination radius by c

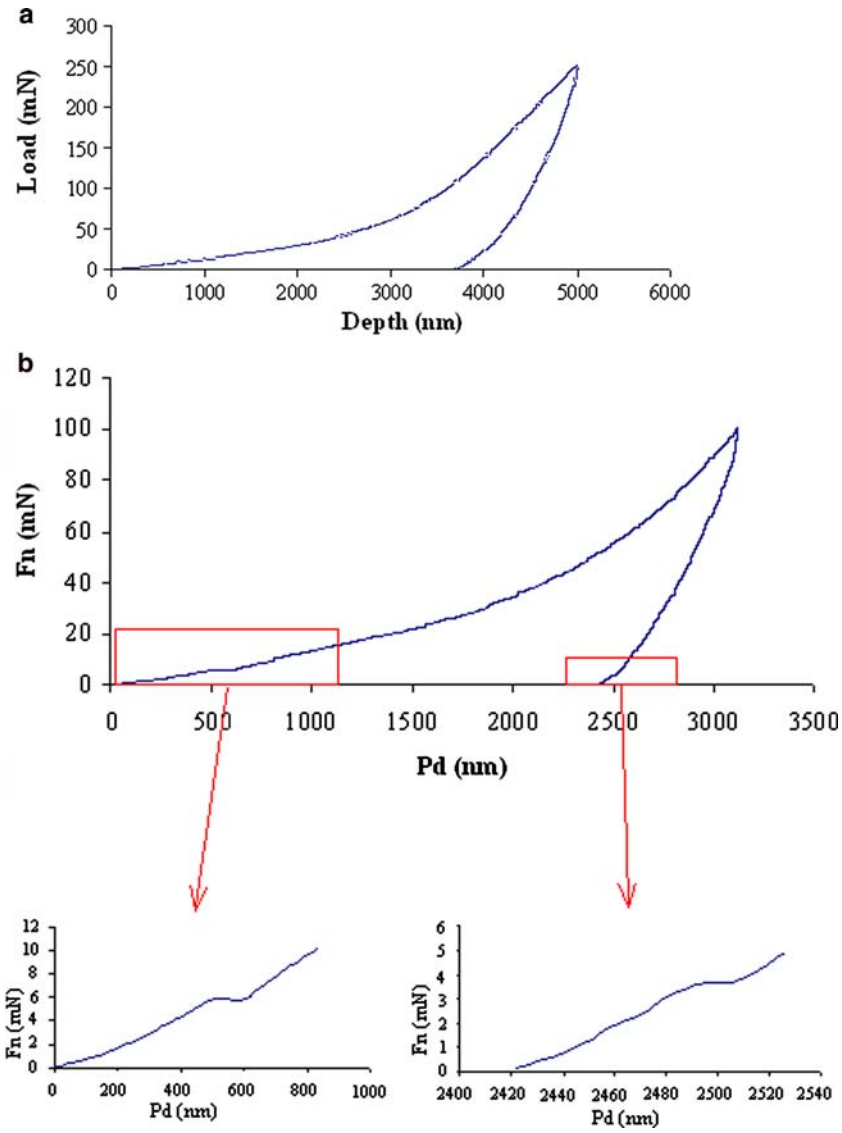


**Fig. 6** (**a**) Typical load-displacement curve obtained from a delamination indentation using a load of 250 mN and a loading rate of 500 mN/min. (**b**) Typical load-displacement curve obtained from a delamination indentation using a load of 100 mN and a loading rate of 200 mN/min. The boxed areas on the main graph show where the discontinuities occur on the loading and unloading portion of the curve, while the two graphs below are the enlarged version of the areas in question. The enlarged area on the left shows when the delamination occurs, while the enlarged area on the right shows where "pop out " occurs

beneath the indenter. Since the indenter tip was quite large (10 μm) there would be a large amount of material compressed under the indenter. As the indenter was removed this material recovered and popped up, pushing against the tip and forcing it up suddenly. This was recorded on the load displacement curve as a discontinuity on the unloading curve. The reason these irregularities were observed when a load of 100 mN was used and not when 250 mN was used, was probably because with a load of 250 mN the tip was loaded at a rate of 500 mN/min. At this loading rate, the sensitivity was too low to detect and record the slight changes in the loading and unloading curve that correspond to delamination. When this indentation was repeated at 100 mN the loading rate was 200 mN/min. This was a significantly slower loading rate than previously and allowed for more accurate and sensitive recording of the load-displacement curve.

### 3.5 Influence of surface roughness on the interfacial fracture toughness

Table 2 shows the different adhesion strengths that were obtained for the different wire samples. The surface treatments the wires received clearly had an affect on the fracture toughness. The main factor changed by the surface treatments was the surface roughness, suggesting that the surface roughness is a parameter that needs to be considered when studying adhesion energies. It has previously been reported that surface parameters such as roughness and chemistry can influence adhesion at interfaces [5]. One previous study has suggested that for moderately rough surfaces, an increase in surface area may lead to a proportionate increase in adhesive strength. This may be true as along as the roughness is not great enough to reduce contact between the surfaces [7].

Sample No.1, which was etched, had an $R_z$ roughness of 278 nm and the fracture toughness was calculated as 0.32 $Jm^{-2}$. Sample No.5, which was etched, as with sample No.1 but subsequently mechanically polished, had a roughness of 92 nm and fracture toughness of 0.19 $Jm^{-2}$. The mechanical polishing reduced the surface roughness and there was also a clear reduction in the measured fracture toughness. Sample No.3, which was etched and pickled, had an $R_z$ roughness of 230 nm and fracture toughness of 0.20 $Jm^{-2}$. Sample No.4 was etched and pickled but also mechanically polished. This sample had an $R_z$ value of 145 nm and a fracture toughness of 0.10 $Jm^{-2}$. Again the mechanical polishing process reduced the surface roughness, which resulted in a reduction in the calculated fracture toughness. It appears from the results obtained that the smoother surfaces, with lower roughness values, have the lowest interfacial fracture toughness. This trend is also seen when sample 2 and sample 4 are compared.

Samples No.4 and No.5 show an exception to the trend of lower roughness resulting in lower fracture toughness. No.4 has an $R_z$ roughness of 145 nm and fracture toughness of 0.10 $Jm^{-2}$, while No.5 has a roughness of 92 nm and fracture toughness of 0.19 $Jm^{-2}$. It may be the case that the surface chemistry and surface energy of the wire samples is altered by the various surface treatments the wires received, and not just the surface roughness, which was examined in this study. As mentioned already surface chemistry and energy can affect adhesion at interfaces [5]. While it was possible to analyse the affect of surface roughness on the adhesive strength, it was not possible to study the influence of the individual surface treatments, as these procedures were carried out at the site of manufacture. The results of this study show that the polymer adhesion is dependant on the surface roughness. The surface roughness of the substrate is, therefore, an important parameter that must be considered when studying adhesion between coatings and substrates. However, other parameters, such as, surface chemistry and surface energy must also be considered. Overall, our results agree with previous studies that suggest substrate roughness has an affect on the strength of adhesion when films are coated to substrates [5, 7].

## 4 Conclusion

An established method, previously used to measure the adhesive strength between films on flat substrates, has now being successfully employed for measuring the adhesion between films and wire substrates that have received various surface treatments. Results indicate that the surface roughness is an important factor that affects the strength of adhesion, with the general trend being an increase in the adhesive strength as the roughness increases. The greater surface area available on the rougher samples for adhesion between the polymer and substrate may account for this relationship. Therefore, the planar model used in this study is not completely sufficient for describing materials with relatively rough surface, as the roughness is not taken into account when calculating the interfacial fracture toughness. These results now allow for the further development of a more complete model for the analysis of the strength of adhesion between polymers and wire substrates, and possibly stents, which is of great importance when evaluating their biocompatibility. Our values quoted in Table 2 are typical for values measured for thin films on rigid substrates. As a comparison, Li et al have reported values in the range 0.6 $Jm^{-2}$ for polystyrene films on glass substrates [2]. Our results are in agreement with the idea that roughness can significantly influence adhesion at interfaces. Thus, for the polymer system used in this study it appears that the coating adherence is at its best when the substrate surface is roughest. Since most stent surfaces are subjected to electropolishing treatments after laser cutting, and while the smoothing of the surface eliminates possible balloon penetration sites and improves fatigue life, it may also lead to premature delamination of the coating, which as stated earlier may affect the biocompatibility of the implant and rate of drug release from the polymer.

**Acknowledgements** Financial support for this study was provided by the Research Council for Science, Engineering and Technology (IRCSET): funded by the national development plan.

## References

1. A. A. VOLINSKY, N. R. MOODY, W. W. GERBERICH, Acta Materialia. **50** (2002) 441–466
2. M. LI, M. L. PALACIO, C. BARRY CARTER, W. W. GERBERICH, *Thin Solid Films.* **416** (2002) 174
3. A. L. LEWIS, S. L. WILLIS, S. A. SMALL, S. R. HUNT, V. O'BYRNE, P. W. STRATFORD, *Bio-Med. Mater. Eng.* **14** (2004) 355
4. N. A. SMITH, G. ANTOUN, A. B. ELLIS, W. C. CRONE, *Composites A.* **35** (2004) 1307
5. A. SCHIRMEISEN, D. WEINER, H. FUCHS, *Surf. Sci.* **545** (2003) 155–162
6. H. Q. LI, X. CAI, Q. L. CHENG, *J. Mater. Sci. Lett.* **20** (2001) 2167–2171
7. D. E. PACKHAM, *Int. J. Adhes. Adhesi.* **23** (2003) 437
8. C. TREPANIER, T. K. LEUNG, M. TABRIZIAN, L. H. YAHIA, J. G. BIENVENU, J. F. TANGUAY, D. L. PIRON, L. BILODEAU, *J. Biomed. Mater. Res.* **48** (1999) 165
9. D. J. WEVER, A. G. VELDHUIZEN, J. DE VRIES, H. J. BUSSCHER, D. R. A. UGES, J. R. VAN HORN, *Biomaterials.* **19** (1998) 761
10. G. RONDELLI, B. VICENTINI, *Biomaterials.* **20** (1990) 785
11. J. RYHANEN, M. KALLIOINEN, J. TUUKKANEN, J. JUNILA, E. NIEMELA, P. SANDVIK, W. SERLO, *J. Biomed. Mater. Res.* **41** (1998) 481

12. J. RYHANEN, M. KALLIOINEN, J. TUUKKANEN, P. LEHENKARI, J. JUNILA, E. NIEMELA, P. SANDVIK, W. SERLO, *Biomaterials* **20** (1999) 1309
13. D. WEVER, A. G. VELDHUIZEN, M. M. SANDERS, J. M. SCHAKENRAAD, J. R. VAN HORN, *Biomaterials* **18** (1997) 1150
14. J. WATAHA, P. E. LOCKWOOD, M. MAREK, M. GHAZI, *J Biomed Mater. Res. 1999* **45** (1999) 251
15. T. LEON YU, W.-C. LU, W.-H. LIU, H.-L. LIN, C.-H. CHIU, *Polymer* **45** (2004) 5579
16. F. EECKMAN, A. J. MOES, K. AMIGHI. *Int. J. Pharm.* (2002) 113
17. K. B. DOORTY, T. A. GOLUBEVA, A. V. GORELOV, Y. A. ROCHEV, L. T. ALLEN, K. A. DAWSON, W. M. GALLAGHER, A. K. KEENAN. *Cardiovasc. Pathol*. (2003) 105
18. C. A. KAVANAGH, Y. A. ROCHEV, W. M. GALLAGHER, K. A. DAWSON, A. K. KEENAN, *Pharmacol. Ther.* **102** (2004) 1
19. L. G. ROSENFELD, J. E. RITTER, T. J. LARDNER, M. R. LIN, *J. Appl. Phys.* **67**(7) (1990) 3291–3296
20. Y. LU, D. M. SHINOZAKI, *J. Mater. Sci.* **37** (2002) 1283
21. J. MALZBENDER, G. DE WITH, *Surf. Coatings Technol.* **135** (2000) 60
22. O. C. OLIVER, G. M. PHARR, *J. Mater. Res.* **7** (1992) 1564
23. G. M. PHARR, W. C. OLIVER, *MRS Bull.* **17** (1992) 28
24. J. QI, K. H. LAI, C. S. LEE, *Diamond relat. mater.* **10** (2001) 1833
25. S. V. HAINSWORTH, M. R. MCGUIRK, T. F. PAGE, *Surf. Coatings Technol.* **102** (1998) 97
26. X. LI, DONGFENG. DIAO, BHARAT. BHUSHAN, *Acta Materialia.* **45** (1997) 4453
27. M. D. KRIESE, D. A. BOISMIER, N. R. MOODY, W. W. GERBERICH, *Eng. Fract. Mech.* **61** (1998) 1–20
28. S. ETIENNE-CALAS, A. DURI, P. ETIENNE, *J. Non-Cryst. Solids* **344** (2004) 60